ACS OMEGA

Open Access

http://pubs.acs.org/journal/acsodf

Article

Structural and Anticancer Studies of Methoxyflavone Derivative from *Strychnos pseudoquina* A.St.-Hil. (Loganiaceae) from Brazilian Cerrado

Marianna C. Silva,* Gracielle Cunha, Pollyana Firmino, Loide O. Sallum, Antônio Menezes, Jocely Dutra, João de Araujo-Neto, Alzir A. Batista, Javier Ellena, and Hamilton B. Napolitano*

Cite This: *ACS Omega* 2023, 8, 40764−40774

Read Online

ACCESS | Metrics & More | Article Recommendations | Supporting Information

ABSTRACT: The Cerrado biome is the world's largest and most diversified tropical savanna. Despite its diversity, there remains a paucity of scientific discussion and evidence about the medicinal use of Cerrado plants. One of the greatest challenges is the complexity of secondary metabolites, such as flavonoids, present in those plants and their extraction, purification, and characterization, which involves a wide range of approaches, tools, and techniques. Notwithstanding these difficulties, the search for accurately proven medicinal plants against cancer, a leading cause of death worldwide, has contributed to this growing area of research. This study set out to extract, purify, and characterize 3-*O*-methylquercetin isolated from the plant *Strychnos pseudoquina* A.St.-Hil. (Loganiaceae) and to test it for antiproliferative activity and selectivity against different tumor and nontumor human cell lines. A combined-method approach was employed using ^{1}H and ^{13}C nuclear magnetic resonance, thermogravimetric analysis, differential scanning calorimetry, single-crystal X-ray diffraction, Hirshfeld surface analysis, and theoretical calculations to extensively characterize this bioflavonoid. 3-*O*-methylquercetin melts around 275 °C and crystallizes in a nonplanar conformation with an angle of 18.02° between the pyran ring (C) and the phenyl ring (B), unlike quercetin and luteolin, which are planar. Finally, the in vitro cytotoxicity of 3-*O*-methylquercetin was compared with data from quercetin, luteolin, and cisplatin, showing that structural differences influenced the antiproliferative activity and the selectivity against different tumor cell lines.

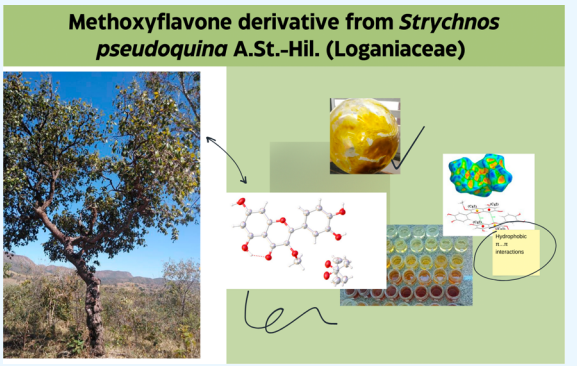

INTRODUCTION

The Cerrado is the second largest biome in Brazil by area and the world's richest savanna in terms of biodiversity.[1,2] Its high degree of endemism and the loss of its native area of approximately 46%, due to agricultural expansion processes, have made it one of the 34 hot spots for conservation in the world.[3,4] Among the species of native Cerrado plants, *Strychnos pseudoquina* stands out, popularly known as "quina-do-cerrado".[5−7] Regarding phytochemical studies using *S. pseudoquina*, the presence of secondary metabolites such as alkaloids and flavonoids is normally demonstrated, and their occurrence is explained by soil conditions, frequent fires, and water stress existing in the Cerrado.[4,8−12]

The therapeutic potential of native Cerrado plants is due to the presence of secondary metabolites, such as flavonoids, which are evidenced through phytochemical studies; their occurrence is favored by the conditions of altitude, soil, and relief present in this biome. These compounds have several pharmacological properties, which are influenced by their structural variations. Flavonoids represent a diverse class of metabolites, with about 5000 known compounds, which can be classified into flavonols, flavones, flavonones, isoflavones, anthocyanins, and chalcones, all derived from the basic structure of 1,3-diphenylpropan-1-one (C6−C3−C6).[13−15] Their pharmacological properties, such as anti-inflammatory,[16−22] antioxidant,[23−28] antibacterial,[29−33] and antifungal,[34−39] are directly related to their structures.[40,41] Moreover, the biological activities of natural compounds can be influenced by the presence of diverse functional groups, such as methyl or methoxy substituents, which present anticancer activity when compared to flavones with only hydroxy groups. In addition, the presence of the methoxyl group modulates the lipophilicity, influencing the bioavailability, i.e., absorption and distribution processes of a drug.[41,42]

One of the structural variations studied in flavonoids is the presence of substituents at position 3 (R in Figure 1) of ring C,

Received: August 8, 2023
Accepted: October 3, 2023
Published: October 18, 2023

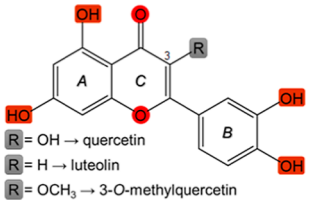

Figure 1. Chemical structure of the flavonoids quercetin, luteolin, and 3-*O*-methylquercetin.

with quercetin and luteolin being the representatives of the flavone group (Figure 1). These natural flavones are considered a strong starting point for the development of anticancer agents, as they can alleviate inflammation, inhibit the proliferation, migration, and invasion of cancer cells, and induce malignant cell death through mechanisms such as apoptosis and autophagy. For instance, when administered with conventional chemotherapy, luteolin has been proven to enhance anticancer effects.[43−46]

Figure 1 illustrates the structure of 3-*O*-methylquercetin, which belongs to the intriguing class of flavonoids and features a methoxy group at the 3-position of ring C. Notably, this flavonoid has previously been identified as a secondary metabolite in various plant species, including the noteworthy presence in *S. pseudoquina* A.St.-Hil from the Loganiaceae family. Recent scientific research has unveiled its multifaceted biological activities, as it has been found to exhibit both antileishmanial and antitumor properties (against breast and lung cancer cells).[47] Furthermore, these recent investigations have not only confirmed its potential but also shed light on its promising in vitro capacity to hinder tumor growth, and this makes 3-*O*-methylquercetin a compelling subject for research.[48] The elucidation of its intricate molecular mechanisms and further research into its pharmacokinetics and safety profile may provide valuable insights into its broader applicability in the field of oncology.

In this article, we report the isolation of 3-*O*-methylquercetin from the stem barks of *S. pseudoquina* and its extensive characterization using spectroscopic techniques, thermal methods, and unprecedented X-ray diffraction. Hirshfeld surface (HS), frontier molecular orbital (FMO) analysis, and a molecular electrostatic potential (MEP) map were also used to investigate the geometric, topological, and electronic structure parameters. Finally, the cytotoxicity and selectivity of the title compound were evaluated against MDA-MB-231, A549, A2780cis, MCF-10A, and MRC-5 cell lines in terms of half-maximal inhibitory concentration (IC_{50}) and selectivity index (Supporting Information).

EXPERIMENTAL AND COMPUTATIONAL PROCEDURES

Plant Material. Bark from the stem of *S. pseudoquina* A.St.-Hil. (Loganiaceae) was collected in Niquelândia, Goiás state, Brazil, in March 2021 (latitude 14°23′33.5″ S, longitude 47°55′37.8″ W). A voucher specimen (14.494) was deposited in the Herbarium of the State University of Goiás (HUEG). Access to the genetic heritage was registered in SisGen under the code A36DDE3.

Extraction and Isolation. The botanical material was dried in an air circulation oven at 45 °C for 48 h and pulverized in a knife mill. The powder (1157 g) was extracted with ethanol 96% at room temperature. The extracted liquid was filtered and concentrated in a rotary evaporator to provide the crude ethanolic extract (122 g). The ethanolic extract was fractionated by vacuum filtration with the incorporation of microcrystalline cellulose D and passing of hexane, ethyl acetate, and methanol to yield the respective fractions: hexane (2.6 g), ethyl acetate (66.6 g), and methanolic (52.2 g) fractions. The ethyl acetate fraction (30 g) was fractioned on a silica gel column (200−400 mesh, 5.0 × 18.0 cm) eluted with CH_2Cl_2/MeOH (gradient: 2, 3, 5, 10, 20, 30, 40, 50%) to yield, after recrystallization with acetone, pure 3-*O*-methylquercetin.

Thermal Analysis. Thermogravimetric analysis (TGA) was performed on Shimadzu TGA-50 equipment. Approximately 3.0 mg ± 0.001 mg were placed in a ceramic (alumina) container and heated at a rate of 10 °C/min under an atmosphere of N_2 (50 mL/min) at 25−400 °C. For differential scanning calorimetry (DSC), a Shimadzu DSC-60 calorimeter was used with 2.0 mg ± 0.02 mg of the sample heated at a rate of 10 °C/min in a sealed aluminum pan. The N_2 flow was also 50 mL/min. Hot-stage microscopy (HSM) was performed by using polarized optical microscopy (Leica DM2500P) equipped with a Linkam hot-stage T95-PE connected to the LNP-95 temperature controller. The sample was heated with a ramp of 10 °C/min, in agreement with DSC and TGA.

Structural Characterization. Nuclear magnetic resonance (NMR) analyses were performed in 11.75 T Bruker equipment (500 MHz), AVANCE III model. The ^{1}H and ^{13}C chemical shifts were acquired with acetone-d_6 as the deuterated solvent and with tetramethylsilane (TMS) as the internal standard. Chemical shifts (δ) are reported in parts per million (ppm). Single crystals were chosen for the X-ray diffraction experiment that was performed at 293 K on an automatic diffractometer Rigaku XtaLAB mini diffractometer (graphite monochromator) with MoKα radiation (λ = 0.71073 Å). CrysAlis^{Pro} (Oxford Diffraction, Agilent Technologies UK Ltd., Yarnton, England) was used for data collection, cell refinement, data reduction, and multiscan method absorption correction. The structure was solved and refined using the SHELX software package,[49,50] hosted in the Olex2 suite.[51] All atoms, except hydrogen, were identified and refined by least-squares full matrix F^2 with anisotropic thermal parameters. The crystallographic tables and the structure representations were generated by Olex2.

Hirshfeld Surface Analysis and Theoretical Calculation. The HS was generated from the program CrystalExplorer[52] and used to evaluate the intermolecular interactions through mapping in color scale. The d_{norm} surface evaluates the distances between the nucleus of the internal atoms to the HS (d_i) and the distance between an external nucleus to the HS (d_e), indicating the donor and acceptor regions, respectively, normalized by the van der Waals (vdW) radius[53] (eq 1)

$$d_{norm} = (d_i - r_i^{vdw})/r_i^{vdw} + (d_e - r_e^{vdw})/r_e^{vdw} \quad (1)$$

where r^{vdw} is the vdW radius. The shape index map was used to describe the interactions, allowing the identification of the characteristic packing modes of the compound and demonstrating the complementarity between the molecules.[54] The contribution of each interaction to the crystalline packing and their respective percentages were provided through the fingerprint, using a standard of 0.6−2.8 Å d_e vs d_i.[55,56]

All density functional theory (DFT) calculations on the 3-*O*-methylquercetin molecule were performed with the Gaussian 16[57] program package. Geometries were fully optimized in the

https://doi.org/10.1021/acsomega.3c05841
ACS Omega 2023, 8, 40764−40774

gas phase from the crystallographic geometry and without symmetry constraints, employing the exchange−correlation functional M062X and basis set 6-311++G(d,p),[58] which has been recommended to treat noncovalent interactions.[59,60]

A relaxed potential energy surface scan was also performed at the same level of theory without any symmetry constraints. Vibrational frequencies were also calculated to classify the critical points as the maximum, minimum, or saddle points of the corresponding potential energy surface. Electronic properties such as the highest occupied molecular orbital (HOMO), the lowest unoccupied molecular orbital (LUMO), excited states [using time-dependent density functional theory (TD-DFT) in the Tamm−Dancoff approximation—TDA], and the MEP were also investigated.[61]

Cell Culture and Viability Assay. The cell lines employed in these assays were the human breast tumor cell lines MDA-MB-231 (ATCC no. HTB-26) and MCF-7 (ATCC no. HTB-22), lung tumor cell line A549 (ATCC no. CCl-185), cisplatin-resistant ovarian tumor cell line A2780cis (Sigma 93112517), and the nontumor human breast and lung cell lines MCF-10A (ATCC no. CRL-10317) and MRC-5 (ATCC no. CCL-171), respectively. The cells were routinely maintained at 37 °C in humidified 5% CO_2 in Dulbecco's Modified Eagle Medium (DMEM) containing fetal bovine serum (FBS) (10%) (MDA-MB-231, A549, and MRC-5), Roswell Park Memorial Institute 1640 medium (RPMI 1640) containing FBS 10% (MCF-7 and A2780cis), DMEM/F12 medium containing horse serum (HS) (5%), epidermal growth factor (EGF—0.02 mg/mL), hydrocortisone (0.05 mg/mL), cholera toxin (0.001 mg/mL), and insulin (0.01 mg/mL) (MCF-10A). All media contained penicillin (100 UI/mL), streptomycin (100 mg/mL), and L-glutamine (2 mM). For the cell viability, 1.5×10^4 cells/well were seeded in 150 μL of complete medium in 96-well plates (Corning Costar) and incubated at 37 °C under 5% CO_2 for 24 h to allow adhesion. After that, 3-*O*-methylquercetin was dissolved in DMSO and 0.75 μL was added per well, resulting in concentrations ranging from 200 to 1.56 μM (0.5% DMSO per well). DMSO does not show toxicity to cells when used at a concentration of 0.5%.[62,63]

The cells were incubated with the compound at 37 °C under 5% CO_2 for 48 h. After that, the MTT [3-(4,5-dimethylthiozol-2-yl)-2,5-diphenyltetrazolium bromide] solution (1 mg mL^{-1}, 50 μL per well) was added to the cells, and the cells were incubated for 3 h. Next, 150 μL of isopropyl alcohol was added to dissolve the precipitated formazan crystals. The maximum final concentration used in the assay was 200 μM in 0.5% DMSO. MTT conversion to formazan by metabolically viable cells was measured on an automated microplate reader at 540 nm. The viability rate in the control wells (cells receiving only DMSO) was taken as a reference (100%) of the cell viability, and the viability rates of the treated cultures were expressed as a percentage of the control value. The percentage of cell viability was plotted against the drug concentration (logarithmic scale) to determine IC_{50} (the drug concentration at which 50% of the cells are viable relative to the control). The error was estimated from the average of three trials by Hill's equation in the GraphPad Prism 9.0 software.

RESULTS AND DISCUSSION

Solid-State Characterization. Thermal analysis has several applications, including purity assessment, identification of polymorphism, stability testing, and thermal decomposition analysis of drugs and compounds.[64] TGA is employed to measure the changes in mass as a function of temperature under controlled atmospheric conditions.[64] It is used for characterizing substances, determining purity and moisture content, identifying polymorphs, and evaluating compound stability. The DSC measures the heat flow of a substance and is useful for purity determination and thermal characterization. It is also effective in detecting polymorphic changes. For a visual understanding, HSM can be conducted to observe the changes in single crystals as the temperature increases.[64]

The thermal profile of 3-*O*-methylquercetin is shown in Figure 2. The crystalline structure exhibited thermal stability

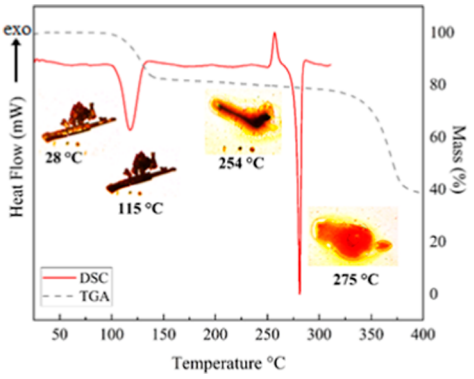

Figure 2. DSC and TGA curves with HSM agreement for the 3-*O*-methylquercetin compound.

up to 115.0 (2) °C, where the output of the acetone molecule is observed to be linked to the first DSC peak (red curve in Figure 2). This observation was confirmed by HSM, which revealed a morphological change caused by the release of the solvent and a mass loss of approximately 20%, as shown by the TGA curve. At 254 (2) °C, the DSC exhibited an exothermic peak followed by one intense endothermic peak, indicating high sample purity during the complete fusion of the compound at 275 (2) °C, which remained stable until 330 (2) °C. At this temperature, the degradation process of the pure compound 3-*O*-methylquercetin begins, and the mass loss is observed on the TGA curve.

Unlike quercetin, which does not simply melt, but for which decomposition and melting occur at overlapping ranges (150−350 °C),[65,66] 3-*O*-methylquercetin melts without decomposition, with the melting confirmed by simultaneous TGA and DSC curves analysis.

The ^{1}H NMR spectrum of 3-*O*-methylquercetin (Figures S1 and S2) showed one methoxyl group at δ 3.87 (3H, *s*, OCH_3-3), and the signals of quercetin at δ 12.82 (1H, *s*, OH-5),7.71 (1H, *d*, J = 2.7 Hz, H-2′), 7.58 (1H, dd, J = 2.7, 10.6 Hz, H-6′), 6.99 (1H, *d*, J = 10.6 Hz, H-5′), 6.50 (1H, *d*, J = 2.6 Hz, H-8), and 6.26 (1H, *d*, J = 2.6 Hz, H-6). This was confirmed by the ^{13}C NMR spectrum (Figure S3), which exhibited 16 carbon signals at δ 155.8 (C-2), 138.3 (C-3), 178.6 (C-4), 162.3 (C-5), 98.5 (C-6), 164.0 (C-7), 93.5 (C-8), 156.9 (C-9), 104.9 (C10), 122.1 (C-1′), 115.4 (C-2′), 144.9 (C-3′), 148.2 (C-4′), 115.4 (C-5′), 121.2 (C-6′), and 59.3 (OCH_3-3′). The NMR data of 3-*O*-methylquercetin were identical with those described in the literature,[67] which was confirmed by the 2D NMR (Figures S4 and S5).

The crystallographic parameters and structural refinements are presented in Table 1. It summarizes the main crystal data collection and structure refinement parameters, which were

https://doi.org/10.1021/acsomega.3c05841
ACS Omega 2023, 8, 40764−40774

Table 1. Crystallographic and Structural Refinement Parameters of 3-*O*-Methylquercetin

empirical formula	$C_{19}H_{12}D_6O_8$
formula weight/g/mol	380.37
temperature/K	293(2)
crystal system	Monoclinic
space group	$P2_1/n$
unit cell dimensions	a = 6.9809(14) Å
	b = 17.360(2) Å
	c = 14.137(2) Å
	β = 90.916(14) °
volume/ Å^3	1713.0(5)
Z'	4
absorption coefficient (μ/mm)	0.114
$F(000)$	784
θ range for data collection	2.754−25.680°
index ranges	$-8 \le h \le 8$, $-21 \le k \le 21$, $-17 \le l \le 17$
reflections collected	13.639
independent reflections	3262 [$R_{(int)}$ = 0.0465]
absorption correction	multiscan
max. and min transmission	0.989 and 0.965
goodness-of-fit on F^2	1.065
final R indices [$I > 2\sigma(I)$]	R_1 = 0.0701, wR_2 = 0.1909
R indices [all data]	R_1 = 0.0995, wR_2 = 0.2388
largest diff. peak and hole/e·Å^{-3}	0.39 and −0.26

deposited under code 2267245 at the Cambridge Crystallographic Data Centre (CCDC). The ORTEP-type diagram (Figure 3) shows the asymmetric unit of 3-*O*-methylquercetin,

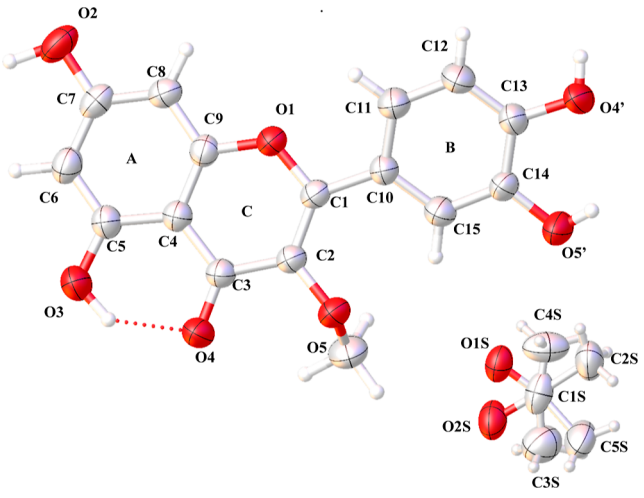

Figure 3. ORTEP-type diagram with 50% probability ellipsoid and atomic numbering scheme of 3-*O*-methylquercetin.

which crystallizes in the monoclinic centrosymmetric space group $P2_1/n$, with one molecule of acetone-d_6. This molecule appears with an occupational disorder for atoms O1S, C1S, C2S, and C3S (50% occupancy) and for atoms O2S, C4S, and C5S (50% of occupancy).

The geometry of the pyran ring in flavones shows planarity due to the double bond between the C1−C2 atoms (1.364 Å), differing from the flavanone compounds in which the pyrone ring has a sofa conformation.[68−74] Although rings A and C lie on the same plane (0.62° between planes), ring B belongs to another plane, which is slightly inclined in relation to the plane of A and C, Figure 4 shows the angle between rings A/C and B (θ1 = 18.02°), evidencing the nonplanarity of the 3-*O*-

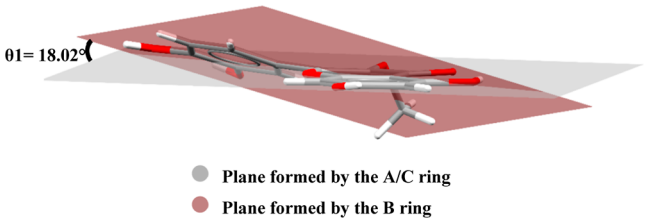

Figure 4. Torsion angle between the least-squares planes through rings A/C and B.

methylquercetin solvate, unlike the crystal structures of related hydroxyflavones quercetin[75,76] and luteolin[77] hydrates.

The dihedral angle C2−C1−C10−C15 (see numbering in Figure 3) is suitable for representing the angle planes through rings A/C and B. In the crystal, this torsion angle is 19.07°. Geometry optimization, M062X//G-311++G(d,p), leads to 27.42°, proving the nonplanar structure. To check if 3-*O*-methylquercetin in the ground state keeps its nonplanarity structure, a relaxed scan of the dihedral angle C2−C1−C10−C15 was performed from 0.0° to 360.0°, and the energy profiles along the scan coordinate are plotted and shown in Figure 5. The dihedral angle C2−C1−C10−C15 is suitable for

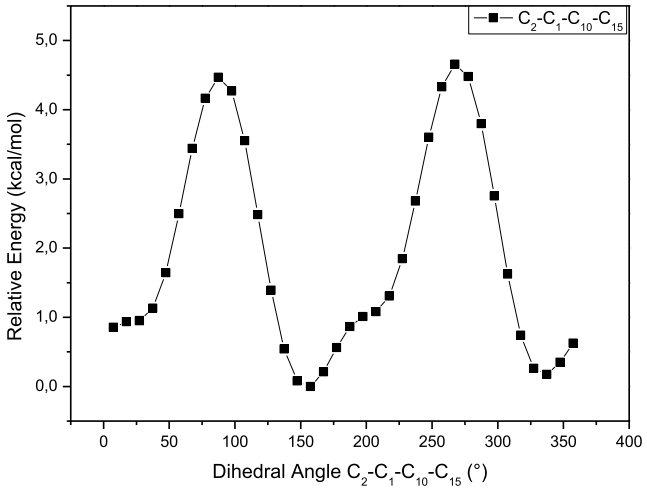

Figure 5. Energy profiles by a relaxed scan of the C2−C1−C10−C15 dihedral of 3-*O*-methylquercetin.

representing the angle planes through rings A/C and B. Around 27° (and 207°) there is a saddle point; i.e., there is one imaginary frequency corresponding to the torsional motion of aromatic ring B directly linked by the C1−C10 bond. This saddle point corresponds to a transition state between the formation and breaking of two simultaneous aligned hydrogen bonds (C15−H−O5 and C11−H−O1). The global maximum is about 87° (and 267°), and the global minimum is around 157° (and 337° or −23°). Figure 5 shows that the total energy difference between the saddle point (at 27°, which corresponds to the same dihedral of the crystallographic structure) and the global minimum (at −23°, which corresponds to a minimum of the potential energy surface) is about 1.0 kcal/mol; i.e., the crystallographic structure and the optimized structure are nearly the same. The small differences probably arise from the

https://doi.org/10.1021/acsomega.3c05841
ACS Omega 2023, 8, 40764−40774

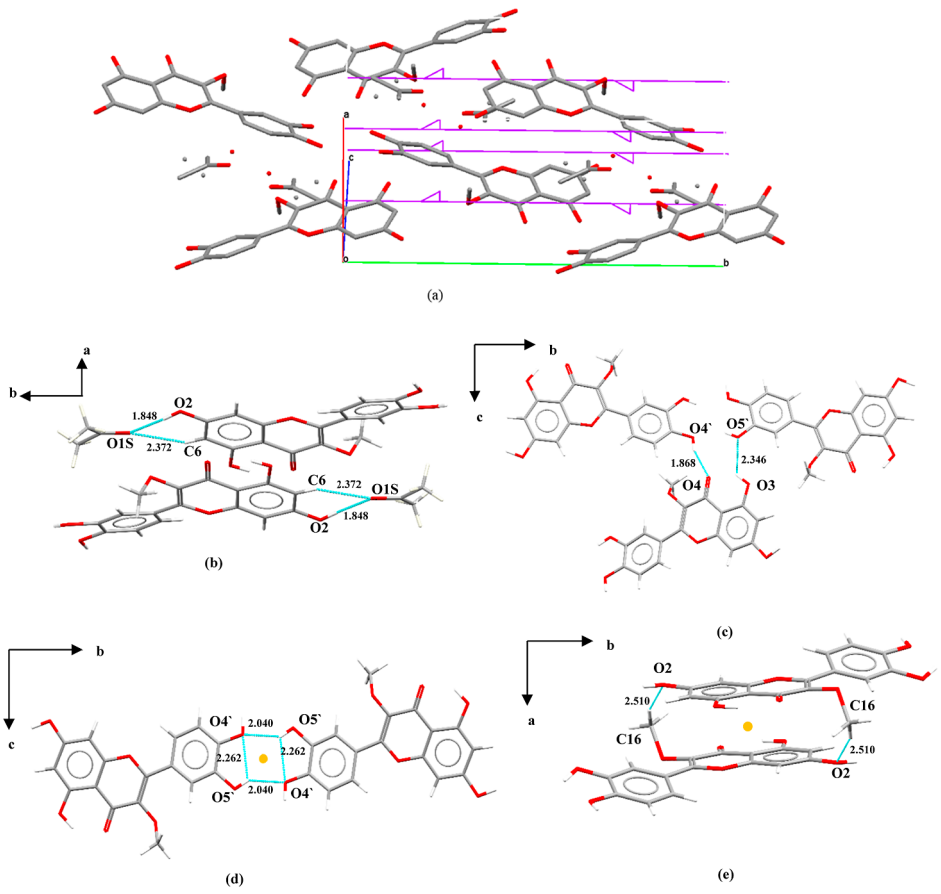

Figure 6. (a) Crystal packing of 3-*O*-methylquercetin (hydrogen atoms have been omitted for clarity). The purple lines show the twofold screw axis. (b−e) Intra- and intermolecular interactions that stabilize the crystal packing. The orange dot represents the inversion center of the compound.

Table 2. Geometric Parameters of the Intra- and Intermolecular Interactions in 3-*O*-Methylquercetin

	D−H···A	D−H/Å	H···A/Å	D···A/Å	D−H···A/degree	symmetry code
3-*O*-methylquercetin	O2−H2···O1S	1.03 (5)	1.85 (5)	2.85 (6)	166 (4)	$-x,1-y,1-z$
	C6−H6···O1S	1.02 (3)	2.37 (3)	3.17 (6)	135 (2)	$-x,1-y,1-z$
	O3−H3···O5′	0.96 (5)	2.35 (4)	3.03 (3)	128 (4)	$1/2-x,1/2+y,1/2-z$
	O4′−H4′···O4	0.82 (4)	1.87 (4)	2.61 (3)	150 (5)	$1/2+x,1/2-y,1/2+z$
	O5′−H5′···O4′	0.83 (5)	2.26 (4)	2.69 (7)	113 (4)	intramolecular
	O5′−H5′···O4′	0.83 (5)	2.04 (5)	2.76 (3)	146 (4)	$1-x,-y,1-z$
	C16−H16B···O2	1.03 (5)	2.51 (5)	3.49 (5)	161 (4)	$1-x,1-y,1-z$

crystal packing interaction, which is not treated in the theoretical calculations.

The crystal packing of 3-*O*-methylquercetin is related to the twofold screw axis parallel to the *b* axis (Figure 6a). Its stabilization occurs through intra- and intermolecular interactions (Table 2). The O1S atom of the acetone-d_6 molecule performs a bifurcated interaction between the O2 and C6 atoms, forming a $R_2^1(6)$ motif parallel to the *b* axis (Figure 6b). The O3−H3···O5′ hydrogen bond forms infinite zigzag chains along the *b* axis with the $C_1^1(11)$ graph set. Similarly, the O4′−H4′···O4 interaction also forms chains that can be described by $C_1^1(10)$ perpendicular to the plane *bc* (Figure 6c). O5′−H5′···O4′ intermolecular interactions form dimers around the inversion center, which can be described as a $R_2^2(10)$ (Figure 6d). Furthermore, C16−H16B···O2 also forms a centrosymmetric dimer that is associated with $R_2^2(20)$ (Figure 6e).

To understand the intermolecular interactions, we performed the analysis of HS d_{norm}, where the distance within the molecule between the external (d_e) and internal (d_i) nucleus of the HS are identified by blue and red spots, respectively. 3-*O*-methylquercetin intermolecular interactions are demonstrated in Figure 7a−d. The hydrophobic $\pi\cdots\pi$ interactions are described by the shape index, where overlapping rings occur, represented by red and blue triangles. The distance between the gravitational centers Cg1 (formed by O1−C1−C2−C3−C4−C9) and Cg2 (formed by C4−C5−C6−C7−C8−C9) is 3.46 Å, which contributes to the additional stability of the three-dimensional arrangement of the compound (Figure 6e). The contribution of each contact present in the molecule is quantified by a fingerprint graph generated from d_e vs d_i. Figure 8 shows the several interaction contributions in the structure of 3-*O*-methylquercetin, with the major contribution to the crystalline packing beginning from the H···H and O···H interactions with 42.1 and 34.0%, respectively, while the C···H

https://doi.org/10.1021/acsomega.3c05841
ACS Omega 2023, 8, 40764−40774

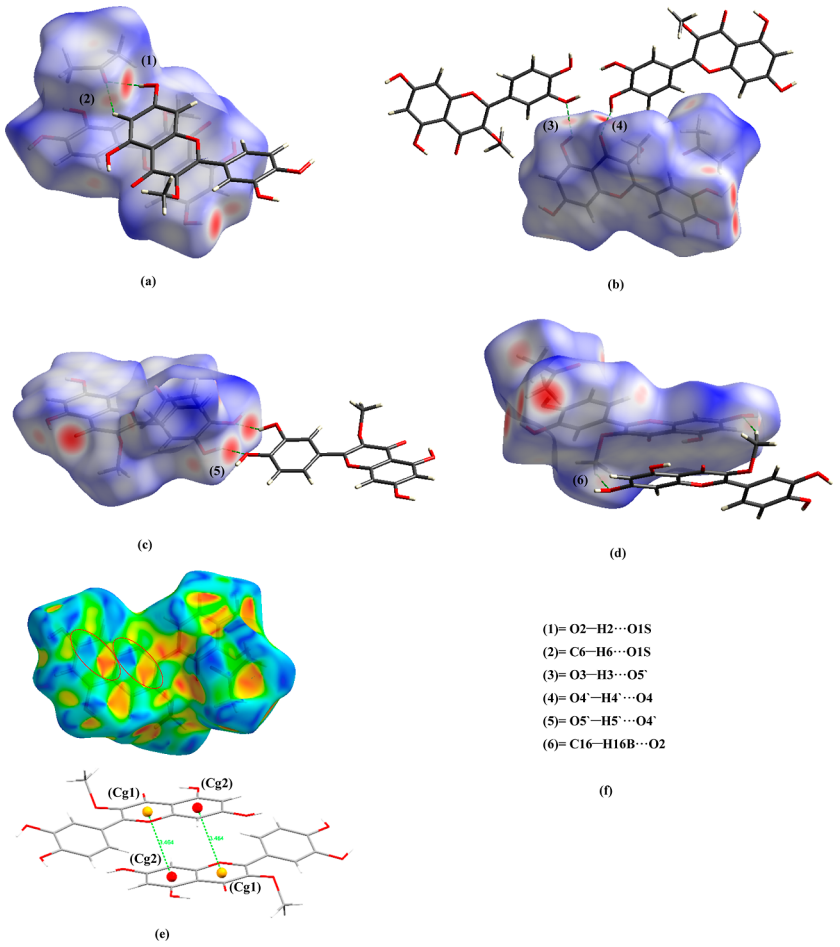

Figure 7. (a–d) HS d_{norm} representing intermolecular contacts for 3-*O*-methylquercetin; and (e) HS shape index showing $\pi\cdots\pi$ interactions for 3-*O*-methylquercetin.

interactions (10.0%) and C···O (7.0%) represent a smaller percentage. The presence of C···C interactions (6.0%) indicates that the packing presents $\pi\cdots\pi$ interactions, which provides additional stability to the structure.

Molecular Modeling Description. The FMO taken from NBO analysis for 3-*O*-methylquercetin were carried out at the M062*X*/6-311+G(d,p) level of theory, and this is shown in Figure 9. The HOMO is localized on the phenyl (B ring), exhibiting an π pure bonding orbital.

The excitation process of 3-*O*-methylquercetin was investigated by means of a TD-DFT method over the optimized geometry fundamental state and using the same M062*X*/6-311+G(d,p) level of theory. The first 10 vertical excitations were calculated (see Table S1). HOMO−LUMO transition (H → L) takes place around 300 nm, which means a HOMO−LUMO gap of 4.1 eV. The absorption spectrum of 3-*O*-methylquercetin is presented in Figure S6. It shows bands with maximum at 300 and 220 nm, which are in agreement with the absorption spectra of typical flavonoids, consisting of band I (300−380 nm) and band II (240−295 nm).[78] The three most intense (greatest oscillator strength) transitions are transitions from HOMO, i.e., the HOMO → LUMO (4.1 eV); the HOMO → LUMO + 1 (5.3 eV); and the HOMO → LUMO + 2 (5.7 eV). Three orbitals contribute to the first excitation (HOMO → LUMO), which are HOMO, HOMO − 1, and HOMO − 4. The second biggest excitation amplitude (HOMO → LUMO + 1) has the major contribution of HOMO, HOMO − 3, and HOMO − 1, while the third one (HOMO → LUMO + 1) has the major contribution of HOMO, HOMO − 1, and HOMO − 2—all those transitions are $\pi \rightarrow \pi^*$.

In Vitro Anticancer Activity. The in vitro cytotoxicity assays on human tumor cell lines represent the standard method for the initial screening of potential antitumor activity of new molecules. To evaluate the 3-*O*-methylquercetin antiproliferative activity, tests were performed on breast (MDA-MB-231), lung (A549), cisplatin-resistant ovary (A2780cis), nontumor breast (MCF-10A), and lung (MRC-5) cell lines. Table 3 presents the IC_{50} values obtained for 3-*O*-methylquercetin and the values described in the literature for quercetin and luteolin (MTT method and 48 h of exposure to flavonoids).

Comparing IC_{50} data obtained from the different cell lines, we see that, in general, 3-*O*-methylquercetin exhibits IC_{50} values of the same order of magnitude as luteolin (<100 μM), while quercetin exhibits high values of IC_{50} (>100 μM). This factor proves that the kind of substituent in position 3 of the C ring can directly influence the in vitro antiproliferative activity of this class of substance. Besides that, the IC_{50} values obtained for the nontumor cells are generally higher than those obtained for the tumor cells, evidencing the low toxicity of the flavonoids for these healthy cell lines. For cisplatin-resistant ovarian cancer (A2780cis), we see that 3-*O*-methylquercetin is slightly more active than cisplatin, while for nontumor cells, 3-

https://doi.org/10.1021/acsomega.3c05841
ACS Omega 2023, 8, 40764−40774

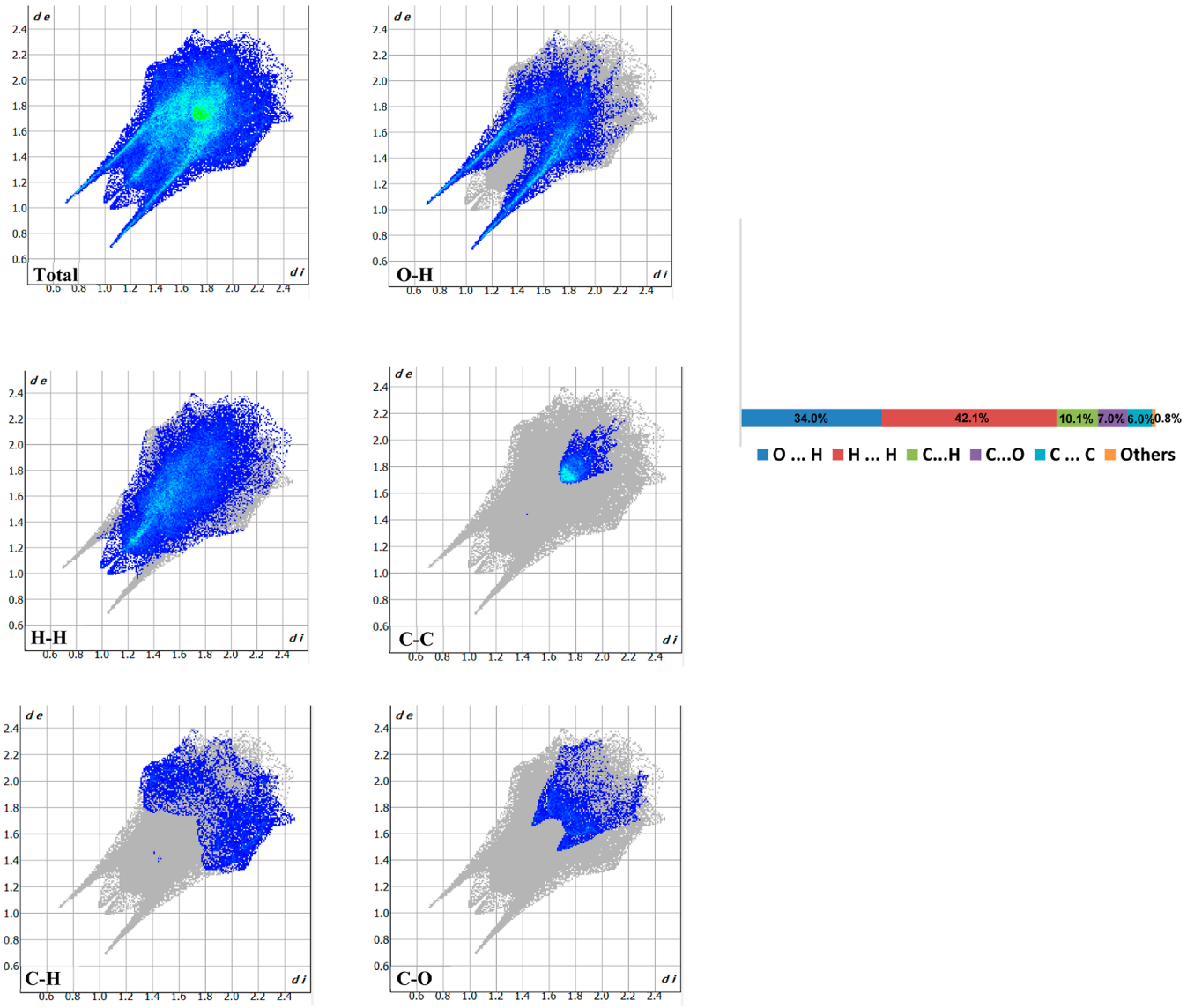

Figure 8. Fingerprint plot quantification of the total interactions in 3-*O*-methylquercetin.

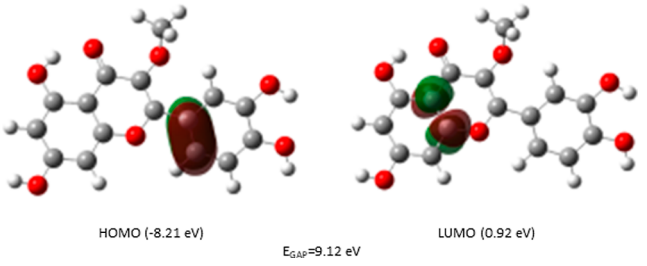

Figure 9. NBO orbitals analysis at the M062*X*/6-311+G(d,p) level of theory with the isovalue of 0.05 atomic units showing the HOMO and the LUMO orbitals, which exhibit the π pure bonding orbital and π pure antibonding orbital, respectively.

O-methylquercetin and quercetin exhibit considerably higher IC_{50} values than cisplatin, which is known to exhibit several side effects, given the low selectivity for tumor tissues.[84] The selectivity values show that 3-*O*-methylquercetin is more selective for breast cancer (>2.2), while quercetin is more selective for lung cancer (>2.2), showing that structural alterations can influence both the antiproliferative activity and the selectivity of flavonoids against different tumor cell lines.

CONCLUSIONS

The present study adds to the growing body of research that indicates that Cerrado plants may be used as a source of potential anticancer compounds. 3-*O*-methylquercetin was extracted and isolated from *S. pseudoquina* A.St.-Hil. (Loganiaceae) using a chromatography technique with a yield of approximately 0.07 mg/g. Characterization of the isolated flavonoids was done by ^{1}H and ^{13}C NMR spectroscopy and by thermal analysis, and its structure was elucidated as belonging to centrosymmetric group space $P2_1/n$, with one molecule of acetone-d6 in the asymmetric unit. The crystal packing is stabilized by O−H···O and C−H···O hydrogen bonds as well as $\pi\cdots\pi$ stacking interactions. HS analysis and shape index map confirmed all the interactions. The substance showed thermal stability until 330 °C, melting point at 275 °C, and chemical stability by possessing a high magnitude of the band gap energy and by showing a UV−vis spectrum with maximum values below 400 nm.

https://doi.org/10.1021/acsomega.3c05841
ACS Omega 2023, 8, 40764−40774

Table 3. IC_{50} Values Were Obtained for 3-*O*-Methylquercetin, Cisplatin, and the Values from the Literature for the Analogues[a,b]

	IC_{50} (μM)			
	quercetin	luteolin	3-*O*-methylquercetin	cisplatin
MDA-MB-231	295[79]	41.9[80]	68.7 ± 0.5	10.23 ± 0.2
A549	100[81]	40.2[82]	68.8 ± 0.5	14.40 ± 1.40
A2780cis			27.4 ± 0.3	37.02 ± 5.10
MCF-10A	178[83]		>150	23.90 ± 0.72
MRC-5	>1000[79]		116.4 ± 0.6	29.90 ± 0.78
	Selectivity Index			
SI_1*	0.6		>2.2	2.3
SI_2**	>2.2		1.7	2.1

[a]All results were obtained employing the MTT colorimetric method with 48 h of exposure of the cells to the flavonoids. [b]SI_1* = IC50 (MCF-10A)/ IC50 (MDA-MB-231) and SI_2* = IC50 (MRC-5)/ IC50 (A549).

Furthermore, the evaluation of cytotoxicity for 3-*O*-methylquercetin, derived from *S. pseudoquina* A.St.-Hil., was juxtaposed with findings from the literature regarding quercetin and luteolin, and this confirms its already reported antitumor efficacy. Quercetin, for instance, displayed IC_{50} values exceeding 100 μM, clearly illustrating how variations in substituents at the 3-position of the C ring exert a significant influence on the antiproliferative activity. This underscores the critical connection between the molecular structure and biological functionality, emphasizing the paramount importance of a comprehensive understanding of the structural attributes of biologically active compounds. More broadly, further research into improving its targeted delivery to cancer tissues is needed using nanotechnological methods or structural alterations and establishing its safety profile in humans. Several strategies, such as structure−activity relationship studies, may aid in the advancement of this path.

■ ASSOCIATED CONTENT

Supporting Information

The Supporting Information is available free of charge at https://pubs.acs.org/doi/10.1021/acsomega.3c05841.

Characterization (^{1}H NMR, ^{13}C NMR, UV−vis); vertical excitation of 3-*O*-methylquercetin; and detailed MEP map results (PDF)

(PDF)

■ AUTHOR INFORMATION

Corresponding Authors

Marianna C. Silva − *Laboratório de Novos Materiais, Universidade Evangélica de Goiás, 75083-515 Anápolis, GO, Brazil*; Email: silva.c.marianna@gmail.com

Hamilton B. Napolitano − *Grupo de Química Teórica e Estrutural de Anápolis, Universidade Estadual de Goiás, 75132-903 Anápolis, GO, Brazil*; orcid.org/0000-0002-6047-9995; Email: hbnapolitano@gmail.com

Authors

Gracielle Cunha − *Laboratório de Produtos Naturais, Universidade Estadual de Goiás, 75132-903 Anápolis, GO, Brazil*

Pollyana Firmino − *Laboratório Multiusuário de Cristalografia Estrutural, Instituto de Física de São Carlos, Universidade de São Paulo, 13566-590 São Carlos, SP, Brazil*

Loide O. Sallum − *Laboratório de Novos Materiais, Universidade Evangélica de Goiás, 75083-515 Anápolis, GO, Brazil*

Antônio Menezes − *Laboratório de Produtos Naturais, Universidade Estadual de Goiás, 75132-903 Anápolis, GO, Brazil*

Jocely Dutra − *Laboratório de Estrutura e Reatividade de Compostos Inorgânicos, Departamento de Química, Universidade Federal de São Carlos, 13565-905 São Carlos, SP, Brazil*

João de Araujo-Neto − *Laboratório de Bioinorgânica, Catálise e Farmacologia, Instituto de Química, Universidade de São Paulo, 05508-000 São Paulo, SP, Brazil*

Alzir A. Batista − *Laboratório de Estrutura e Reatividade de Compostos Inorgânicos, Departamento de Química, Universidade Federal de São Carlos, 13565-905 São Carlos, SP, Brazil*

Javier Ellena − *Laboratório Multiusuário de Cristalografia Estrutural, Instituto de Física de São Carlos, Universidade de São Paulo, 13566-590 São Carlos, SP, Brazil*; orcid.org/0000-0002-0676-3098

Complete contact information is available at: https://pubs.acs.org/10.1021/acsomega.3c05841

Notes

The authors declare no competing financial interest.

■ ACKNOWLEDGMENTS

This research was supported by the Fundação de Amparo à Pesquisa do Estado de Goiás (FAPEG—202110267000521), Conselho Nacional de Desenvolvimento Científico e Tecnológico (CNPq—312505/2021-3 and 160856/2021-3), Fundação de Amparo à Pesquisa do Estado de São Paulo (FAPESP—17/15840-0 and 21/04876-4), and Universidade Estadual de Goiás (UEG—Fomento 45362693; SEI 202200020020883).

■ REFERENCES

(1) Colli, G. R.; Vieira, C. R.; Dianese, J. C. Biodiversity and Conservation of the Cerrado: Recent Advances and Old Challenges. *Biodivers. Conserv.* **2020**, *29* (5), 1465−1475.

(2) Dalle Laste, K. C.; Durigan, G.; Andersen, A. N. Biodiversity Responses to Land-Use and Restoration in a Global Biodiversity Hotspot: Ant Communities in Brazilian Cerrado. *Austral Ecol.* **2019**, *44* (2), 313−326.

(3) Hofmann, G. S.; Cardoso, M. F.; Alves, R. J. V.; Weber, E. J.; Barbosa, A. A.; de Toledo, P. M.; Pontual, F. B.; Salles, L. d. O.;

Hasenack, H.; Cordeiro, J. L. P.; Aquino, F. E.; de Oliveira, L. F. B. The Brazilian Cerrado Is Becoming Hotter and Drier. *Global Change Biol.* **2021**, *27* (17), 4060−4073.
(4) de Brito, G. O.; Reis, B. C.; Ferreira, E. A.; Vilela Junqueira, N. T.; Sá-Barreto, L. C. L.; Mattivi, F.; Vrhovsek, U.; Gris, E. F. Phenolic Compound Profile by UPLC-MS/MS and Encapsulation with Chitosan of Spondias mombin L. Fruit Peel Extract from Cerrado Hotspot—Brazil. *Molecules* **2022**, *27* (8), 2382.
(5) Gontijo, D. C.; Nunes, L. G.; Farias, L. M.; Duarte, M. G. R.; Carvalho, A. F.; Fietto, L. G.; Leite, J. P. V. Assessment of the Phenolic Content, Mutagenicity and Genotoxicity of Ethanolic Extracts of Stem Bark and Leaves from *Strychnos Pseudoquina* A. St.-Hil. *Drug Chem. Toxicol.* **2020**, *43* (5), 539−545.
(6) Boff, L.; Silva, I. T.; Argenta, D. F.; Farias, L. M.; Alvarenga, L. F.; Pádua, R.; Braga, F. C.; Leite, J. P. V.; Kratz, J. M.; Simões, C. *Strychnos Pseudoquina* A. St. Hil.: A Brazilian Medicinal Plant with Promising *in Vitro* Antiherpes Activity. *J. Appl. Microbiol.* **2016**, *121* (6), 1519−1529.
(7) Honório-França, A. C.; Marins, C. M. F.; Boldrini, F.; França, E. L. Evaluation of Hypoglicemic Activity and Healing of Extract from amongst Bark of "Quina Do Cerrado" (Strychnos Pseudoquina ST. HILL). *Acta Cir. Bras.* **2008**, *23* (6), 504−510.
(8) Nicoletti, M.; Goulart, M. O. F.; de Lima, R. A.; Goulart, A. E.; Monache, F. D.; Bettolo, G. B. M. Flavonoids and Alkaloids From Strychnos Pseudoquina. *J. Nat. Prod.* **1984**, *47* (6), 953−957.
(9) de Toledo, T. A.; da Silva, L. E.; Botelho, T. C.; Ramos, R. J.; de Souza, P., Jr.; Teixeira, A. M. R.; Freire, P. T. C.; Bento, R. R. F. Characterization of Flavonoid 3-Methoxyquercetin Performed by FT-IR and FT-Raman Spectroscopies and DFT Calculations. *J. Mol. Struct.* **2012**, *1029*, 22−27.
(10) Bailão, E.; Devilla, I.; da Conceição, E.; Borges, L. Bioactive Compounds Found in Brazilian Cerrado Fruits. *Int. J. Mol. Sci.* **2015**, *16* (10), 23760−23783.
(11) Silva, M.; Duarte, V.; Sallum, L.; Cunha, G.; Custodio, J.; Oliver, A.; Peixoto, J.; Menezes, A.; Napolitano, H. Molecular Modeling Studies of β-Sitosterol Extract from Miconia Burchellii Triana (Melastomataceae) from Brazilian Cerrado. *J. Braz. Chem. Soc.* **2023**, *34* (9), 1293−1302.
(12) Peixoto, J. D. C.; Neves, B. J.; Napolitano, H. B.; Gonçalves, M.; Dutra, S.; Rosseto, L. P. Flavonoids from Brazilian Cerrado: Biosynthesis, Chemical and Biological Profile. *Molecules* **2019**, *24* (16), 2891.
(13) Singh, S.; Gupta, P.; Meena, A.; Luqman, S. Acacetin, a Flavone with Diverse Therapeutic Potential in Cancer, Inflammation, Infections and Other Metabolic Disorders. *Food Chem. Toxicol.* **2020**, *145*, 111708.
(14) Sallum, L. O.; Duarte, V. S.; Custodio, J. M. F.; Faria, E. C. M.; da Silva, A. M.; Lima, R. S.; Camargo, A. J.; Napolitano, H. B. Cyclohexanone-Based Chalcones as Alternatives for Fuel Additives. *ACS Omega* **2022**, *7* (14), 11871−11886.
(15) Yang, G.; Hong, S.; Yang, P.; Sun, Y.; Wang, Y.; Zhang, P.; Jiang, W.; Gu, Y. Discovery of an Ene-Reductase for Initiating Flavone and Flavonol Catabolism in Gut Bacteria. *Nat. Commun.* **2021**, *12* (1), 790.
(16) Maleki, S. J.; Crespo, J. F.; Cabanillas, B. Anti-Inflammatory Effects of Flavonoids. *Food Chem.* **2019**, *299*, 125124.
(17) Kim, H. P.; Son, K. H.; Chang, H. W.; Kang, S. S. Anti-Inflammatory Plant Flavonoids and Cellular Action Mechanisms. *J. Pharmacol. Sci.* **2004**, *96* (3), 229−245.
(18) Serafini, M.; Peluso, I.; Raguzzini, A. Flavonoids as Anti-Inflammatory Agents. *Proc. Nutr. Soc.* **2010**, *69* (3), 273−278.
(19) Spagnuolo, C.; Moccia, S.; Russo, G. L. Anti-Inflammatory Effects of Flavonoids in Neurodegenerative Disorders. *Eur. J. Med. Chem.* **2018**, *153*, 105−115.
(20) García-Lafuente, A.; Guillamón, E.; Villares, A.; Rostagno, M. A.; Martínez, J. A. Flavonoids as Anti-Inflammatory Agents: Implications in Cancer and Cardiovascular Disease. *Inflammation Res.* **2009**, *58* (9), 537−552.
(21) Chen, G.-L.; Fan, M.-X.; Wu, J.-L.; Li, N.; Guo, M.-Q. Antioxidant and Anti-Inflammatory Properties of Flavonoids from Lotus Plumule. *Food Chem.* **2019**, *277*, 706−712.
(22) Fernández-Rojas, B.; Gutiérrez-Venegas, G. Flavonoids Exert Multiple Periodontic Benefits Including Anti-Inflammatory, Periodontal Ligament-Supporting, and Alveolar Bone-Preserving Effects. *Life Sci.* **2018**, *209*, 435−454.
(23) Tungmunnithum, D.; Drouet, S.; Kabra, A.; Hano, C. Enrichment in Antioxidant Flavonoids of Stamen Extracts from Nymphaea Lotus L. Using Ultrasonic-Assisted Extraction and Macroporous Resin Adsorption. *Antioxidants* **2020**, *9* (7), 576.
(24) Wani, T. A.; Bakheit, A. H.; Zargar, S.; Alanazi, Z. S.; Al-Majed, A. A. Influence of Antioxidant Flavonoids Quercetin and Rutin on the In-Vitro Binding of Neratinib to Human Serum Albumin. *Spectrochim. Acta, Part A* **2021**, *246*, 118977.
(25) Agati, G.; Brunetti, C.; Fini, A.; Gori, A.; Guidi, L.; Landi, M.; Sebastiani, F.; Tattini, M. Are Flavonoids Effective Antioxidants in Plants? Twenty Years of Our Investigation. *Antioxidants* **2020**, *9* (11), 1098.
(26) Khan, J.; Deb, P. K.; Priya, S.; Medina, K. D.; Devi, R.; Walode, S. G.; Rudrapal, M. Dietary Flavonoids: Cardioprotective Potential with Antioxidant Effects and Their Pharmacokinetic, Toxicological and Therapeutic Concerns. *Molecules* **2021**, *26* (13), 4021.
(27) Zeng, Y.; Song, J.; Zhang, M.; Wang, H.; Zhang, Y.; Suo, H. Comparison of In Vitro and In Vivo Antioxidant Activities of Six Flavonoids with Similar Structures. *Antioxidants* **2020**, *9* (8), 732.
(28) Wang, Y.; Liu, X.-J.; Chen, J.-B.; Cao, J.-P.; Li, X.; Sun, C.-D. Citrus Flavonoids and Their Antioxidant Evaluation. *Crit. Rev. Food Sci. Nutr.* **2022**, *62* (14), 3833−3854.
(29) Farhadi, F.; Khameneh, B.; Iranshahi, M.; Iranshahy, M. Antibacterial Activity of Flavonoids and Their Structure-Activity Relationship: An Update Review. *Phytother. Res.* **2019**, *33* (1), 13−40.
(30) Shamsudin, N. F.; Ahmed, Q. U.; Mahmood, S.; Ali Shah, S. A.; Khatib, A.; Mukhtar, S.; Alsharif, M. A.; Parveen, H.; Zakaria, Z. A. Antibacterial Effects of Flavonoids and Their Structure-Activity Relationship Study: A Comparative Interpretation. *Molecules* **2022**, *27* (4), 1149.
(31) Adamczak, A.; Ożarowski, M.; Karpiński, T. M. Antibacterial Activity of Some Flavonoids and Organic Acids Widely Distributed in Plants. *J. Clin. Med.* **2019**, *9* (1), 109.
(32) Kurnia, D.; Apriyanti, E.; Soraya, C.; Satari, M. H. Antibacterial Flavonoids Against Oral Bacteria of Enterococcus Faecalis ATCC 29212 from Sarang Semut (Myrmecodia Pendans) and Its Inhibitor Activity Against Enzyme MurA. *Curr. Drug Discovery Technol.* **2019**, *16* (3), 290−296.
(33) Tan, Z.; Deng, J.; Ye, Q.; Zhang, Z. The Antibacterial Activity of Natural-Derived Flavonoids. *Curr. Top. Med. Chem.* **2022**, *22* (12), 1009−1019.
(34) al Aboody, M. S.; Mickymaray, S. Anti-Fungal Efficacy and Mechanisms of Flavonoids. *Antibiotics* **2020**, *9* (2), 45.
(35) Jin, Y.-S. Recent Advances in Natural Antifungal Flavonoids and Their Derivatives. *Bioorg. Med. Chem. Lett.* **2019**, *29* (19), 126589.
(36) Sudheeran, P. K.; Ovadia, R.; Galsarker, O.; Maoz, I.; Sela, N.; Maurer, D.; Feygenberg, O.; Oren Shamir, M.; Alkan, N. Glycosylated Flavonoids: Fruit's Concealed Antifungal Arsenal. *New Phytol.* **2020**, *225* (4), 1788−1798.
(37) Rocha, M. F. G.; Sales, J. A.; da Rocha, M. G.; Galdino, L. M.; de Aguiar, L.; Pereira-Neto, W. d. A.; de Aguiar Cordeiro, R.; Castelo-Branco, D. d. S. C. M.; Sidrim, J. J. C.; Brilhante, R. S. N. Antifungal Effects of the Flavonoids Kaempferol and Quercetin: A Possible Alternative for the Control of Fungal Biofilms. *Biofouling* **2019**, *35* (3), 320−328.
(38) Souza-Moreira, T. M.; Severi, J. A.; Rodrigues, E. R.; de Paula, M. I.; Freitas, J. A.; Vilegas, W.; Pietro, R. C. L. R. Flavonoids from *Plinia Cauliflora* (Mart.) Kausel (Myrtaceae) with Antifungal Activity. *Nat. Prod. Res.* **2019**, *33* (17), 2579−2582.
(39) Al-Huqail, A.; Behiry, S.; Salem, M.; Ali, H.; Siddiqui, M.; Salem, A. A. Antifungal, Antibacterial, and Antioxidant Activities of

https://doi.org/10.1021/acsomega.3c05841
ACS Omega 2023, 8, 40764−40774

Acacia Saligna (Labill.) H. L. Wendl. Flower Extract: HPLC Analysis of Phenolic and Flavonoid Compounds. *Molecules* **2019**, *24* (4), 700.
(40) Panche, A. N.; Diwan, A. D.; Chandra, S. R. Flavonoids: An Overview. *J. Nutr. Sci.* **2016**, *5*, No. e47.
(41) Łużny, M.; Tronina, T.; Kozłowska, E.; Dymarska, M.; Popłoński, J.; Łyczko, J.; Kostrzewa-Susłow, E.; Janeczko, T. Biotransformation of Methoxyflavones by Selected Entomopathogenic Filamentous Fungi. *Int. J. Mol. Sci.* **2020**, *21* (17), 6121.
(42) Waller, M. P.; Hibbs, D. E.; Overgaard, J.; Hanrahan, J. R.; Hambley, T. W. Flavone. *Acta Crystallogr., Sect. E: Struct. Rep. Online* **2003**, *59* (6), o767−o768.
(43) Erdoğan, M. K.; Ağca, C. A.; Aşkın, H. Quercetin and Luteolin Improve the Anticancer Effects of 5-Fluorouracil in Human Colorectal Adenocarcinoma *In Vitro* Model: A Mechanistic Insight. *Nutr. Cancer* **2022**, *74* (2), 660−676.
(44) Seelinger, G.; Merfort, I.; Wölfle, U.; Schempp, C. Anti-Carcinogenic Effects of the Flavonoid Luteolin. *Molecules* **2008**, *13* (10), 2628−2651.
(45) Singh Tuli, H.; Rath, P.; Chauhan, A.; Sak, K.; Aggarwal, D.; Choudhary, R.; Sharma, U.; Vashishth, K.; Sharma, S.; Kumar, M.; Yadav, V.; Singh, T.; Yerer, M. B.; Haque, S. Luteolin, a Potent Anticancer Compound: From Chemistry to Cellular Interactions and Synergetic Perspectives. *Cancers* **2022**, *14* (21), 5373.
(46) Tuli, H. S.; Garg, V. K.; Bhushan, S.; Uttam, V.; Sharma, U.; Jain, A.; Sak, K.; Yadav, V.; Lorenzo, J. M.; Dhama, K.; Behl, T.; Sethi, G. Natural Flavonoids Exhibit Potent Anticancer Activity by Targeting MicroRNAs in Cancer: A Signature Step Hinting towards Clinical Perfection. *Transl. Oncol.* **2023**, *27*, 101596.
(47) Lage, P. S.; de Andrade, P. H. R.; Lopes, A. d. S.; Chávez Fumagalli, M. A.; Valadares, D. G.; Duarte, M. C.; Pagliara Lage, D.; Costa, L. E.; Martins, V. T.; Ribeiro, T. G.; Filho, J. D. d. S.; Tavares, C. A. P.; Pádua, R. M. d.; Leite, J. P. V.; Coelho, E. A. F. *Strychnos Pseudoquina* and Its Purified Compounds Present an Effective *In Vitro* Antileishmanial Activity. *Evidence-Based Complementary Altern. Med.* **2013**, *2013*, 1−9.
(48) Cao, L.; Yang, Y.; Ye, Z.; Lin, B.; Zeng, J.; Li, C.; Liang, T.; Zhou, K.; Li, J. Quercetin-3-methyl Ether Suppresses Human Breast Cancer Stem Cell Formation by Inhibiting the Notch1 and PI3K/Akt Signaling Pathways. *Int. J. Mol. Med.* **2018**, *42*, 1625−1636.
(49) Sheldrick, G. M. *SHELXT* - Integrated Space-Group and Crystal-Structure Determination. *Acta Crystallogr., Sect. A: Found. Adv.* **2015**, *71* (1), 3−8.
(50) Sheldrick, G. M. Crystal Structure Refinement with *SHELXL*. *Acta Crystallogr., Sect. C: Struct. Chem.* **2015**, *71* (1), 3−8.
(51) Puschmann, H.; Bourhis, L. J.; Dolomanov, O. V.; Gildea, R. J.; Howard, J. A. K. *OLEX2* - a Complete Package for Molecular Crystallography. *Acta Crystallogr., Sect. A: Found. Crystallogr.* **2011**, *67* (a1), C593.
(52) Wolff, S. K.; Grimwood, D. J.; McKinnon, J. J.; Turner, M. J.; Jayatilaka, D.; Spackman, M. A. *CrystalExplorer*. version 3.1; University of Western Australia, 2012.
(53) Spackman, M. A.; Jayatilaka, D. Hirshfeld Surface Analysis. *CrystEngComm* **2009**, *11* (1), 19−32.
(54) McKinnon, J. J.; Spackman, M. A.; Mitchell, A. S. Novel Tools for Visualizing and Exploring Intermolecular Interactions in Molecular Crystals. *Acta Crystallogr., Sect. B: Struct. Sci.* **2004**, *60* (6), 627−668.
(55) Spackman, M. A.; Mckinnon, J. J. Fingerprinting Intermolecular Interactions in Molecular Crystals. *CrystEngComm* **2002**, *4* (66), 378−392.
(56) McKinnon, J. J.; Jayatilaka, D.; Spackman, M. A. Towards Quantitative Analysis of Intermolecular Interactions with Hirshfeld Surfaces. *Chem. Commun.* **2007**, No. 37, 3814−3816.
(57) Frisch, M. J.; Trucks, G. W.; Schlegel, H. B.; Scuseria, G. E.; Robb, M. A.; Cheeseman, J. R.; Scalmani, G.; Barone, V.; Petersson, G. A.; Nakatsuji, H.; Li, X.; Caricato, M.; Marenich, A. v.; Bloino, J.; Janesko, B. G.; Gomperts, R.; Mennucci, B.; Hratchian, H. P.; Ortiz, J. v.; Izmaylov, A. F.; Sonnenberg, J. L.; Williams-Young, D.; Ding, F.; Lipparini, F.; Egidi, F.; Goings, J.; Peng, B.; Petrone, A.; Henderson, T.; Ranasinghe, D.; Zakrzewski, V. G.; Gao, J.; Rega, N.; Zheng, G.; Liang, W.; Hada, M.; Ehara, M.; Toyota, K.; Fukuda, R.; Hasegawa, J.; Ishida, M.; Nakajima, T.; Honda, Y.; Kitao, O.; Nakai, H.; Vreven, T.; Throssell, K.; Montgomery, J. A., Jr.; Peralta, J. E.; Ogliaro, F.; Bearpark, M. J.; Heyd, J. J.; Brothers, E. N.; Kudin, K. N.; Staroverov, V. N.; Keith, T. A.; Kobayashi, R.; Normand, J.; Raghavachari, K.; Rendell, A. P.; Burant, J. C.; Iyengar, S. S.; Tomasi, J.; Cossi, M.; Millam, J. M.; Klene, M.; Adamo, C.; Cammi, R.; Ochterski, J. W.; Martin, R. L.; Morokuma, K.; Farkas, O.; Foresman, J. B.; Fox, D. J. *Gaussian 16*; Gaussian, Inc.: Wallingford CT, 2016.
(58) Chai, J.-D.; Head-Gordon, M. Long-Range Corrected Hybrid Density Functionals with Damped Atom-Atom Dispersion Corrections. *Phys. Chem. Chem. Phys.* **2008**, *10* (44), 6615.
(59) Zhao, Y.; Truhlar, D. G. The M06 Suite of Density Functionals for Main Group Thermochemistry, Thermochemical Kinetics, Noncovalent Interactions, Excited States, and Transition Elements: Two New Functionals and Systematic Testing of Four M06-Class Functionals and 12 Other Functionals. *Theor. Chem. Acc.* **2008**, *120* (1−3), 215−241.
(60) Mardirossian, N.; Head-Gordon, M. How Accurate Are the Minnesota Density Functionals for Noncovalent Interactions, Isomerization Energies, Thermochemistry, and Barrier Heights Involving Molecules Composed of Main-Group Elements? *J. Chem. Theory Comput.* **2016**, *12* (9), 4303−4325.
(61) Pyykkö, P. Valency and Bonding. A Natural Bond Orbital Donor-Acceptor Perspective. Von Frank Weinhold Und Clark Landis. *Angew. Chem.* **2006**, *118* (1), 28−29.
(62) Jamalzadeh, L.; Ghafoori, H.; Sariri, R.; Rabuti, H.; Nasirzade, J.; Hasani, H.; Aghamaali, M. R. Cytotoxic Effects of Some Common Organic Solvents on MCF-7, RAW-264.7 and Human Umbilical Vein Endothelial Cells. *Avicenna J. Med. Biochem.* **2016**, *4* (1), 10-33453. In press (In press)
(63) Timm, M.; Saaby, L.; Moesby, L.; Hansen, E. W. Considerations regarding use of solvents in in vitro cell based assays. *Cytotechnology* **2013**, *65* (5), 887−894.
(64) de Oliveira, M. A.; Yoshida, M. I.; Lima Gomes, E. C. de. Análise Térmica Aplicada a Fármacos e Formulações Farmacêuticas Na Indústria Farmacêutica. *Quim. Nova* **2011**, *34* (7), 1224−1230.
(65) da Costa, E. M.; Filho, J. M. B.; do Nascimento, T. G.; Macêdo, R. O. Thermal Characterization of the Quercetin and Rutin Flavonoids. *Thermochim. Acta* **2002**, *392*−*393*, 79−84.
(66) Tsioptsias, C.; Tsivintzelis, I. On the Thermodynamic Thermal Properties of Quercetin and Similar Pharmaceuticals. *Molecules* **2022**, *27* (19), 6630.
(67) Markham, K. R. Flavones, Flavonols, and Their Glycosides. *Methods Plant Biochem.* **1989**, *1*, 197−235.
(68) Redzynia, I.; Ziółkowska, N.; Majzner, W.; Willför, S.; Sjöholm, R.; Eklund, P.; Bujacz, G. Structural Investigation of Biologically Active Phenolic Compounds Isolated from European Tree Species. *Molecules* **2009**, *14* (10), 4147−4158.
(69) Nesterov, V. v.; Zakharov, L. N.; Nesterov, V. N.; Calderon, J. G.; Longo, A.; Zaman, K.; Choudhury, F. K.; Farrell, W.; Shulaev, V.; Richmond, M. G. 5,7-Dihydroxy-2-(4-Hydroxyphenyl)Chroman-4-One (Naringenin): X-Ray Diffraction Structures of the Naringenin Enantiomers and DFT Evaluation of the Preferred Ground-State Structures and Thermodynamics for Racemization. *J. Mol. Struct.* **2017**, *1130*, 994−1000.
(70) dos S. Grecco, S.; Dorigueto, A.; Landre, I.; Soares, M.; Martho, K.; Lima, R.; Pascon, R.; Vallim, M.; Capello, T.; Romoff, P.; Sartorelli, P.; Lago, J. Structural Crystalline Characterization of Sakuranetin — An Antimicrobial Flavanone from Twigs of Baccharis Retusa (Asteraceae). *Molecules* **2014**, *19* (6), 7528−7542.
(71) Shoja, M. 4',5-Dihydroxy-7-Methoxyflavanone. *Acta Crystallogr., Sect. C: Struct. Chem.* **1990**, *46* (10), 1969−1971.
(72) Shin, W.; Lah, M. S. Structure of (R, S)-Naringenin. *Acta Crystallogr., Sect. C: Struct. Chem.* **1986**, *42* (5), 626−628.
(73) Wu, H.; Xu, Z.; Zhou, J.; Liang, Y.-M. 2-(2,3-Dimethoxyphenyl)Chroman-4-One. *Acta Crystallogr., Sect. E: Struct. Rep. Online* **2005**, *61* (4), o1095−o1096.

https://doi.org/10.1021/acsomega.3c05841
ACS Omega 2023, 8, 40764−40774

(74) Shin, W.; Kim, S.; Chun, K. S. Structure of (R, S)-Hesperetin Monohydrate. *Acta Crystallogr., Sect. C: Struct. Chem.* **1987**, *43* (10), 1946−1949.
(75) Domagała, S.; Munshi, P.; Ahmed, M.; Guillot, B.; Jelsch, C. Structural Analysis and Multipole Modelling of Quercetin Monohydrate - a Quantitative and Comparative Study. *Acta Crystallogr., Sect. B: Struct. Sci.* **2011**, *67* (1), 63−78.
(76) Rossi, M.; Rickles, L. F.; Halpin, W. A. The Crystal and Molecular Structure of Quercetin: A Biologically Active and Naturally Occurring Flavonoid. *Bioorg. Chem.* **1986**, *14* (1), 55−69.
(77) Cox, P. J.; Kumarasamy, Y.; Nahar, L.; Sarker, S. D.; Shoeb, M. Luteolin. *Acta Crystallogr., Sect. E: Struct. Rep. Online* **2003**, *59* (7), o975−o977.
(78) Taniguchi, M.; LaRocca, C. A.; Bernat, J. D.; Lindsey, J. S. Digital Database of Absorption Spectra of Diverse Flavonoids Enables Structural Comparisons and Quantitative Evaluations. *J. Nat. Prod.* **2023**, *86* (4), 1087−1119.
(79) Roshanazadeh, M.; Babaahmadi Rezaei, H.; Rashidi, M. Quercetin Synergistically Potentiates the Anti-Metastatic Effect of 5-Fluorouracil on the MDA-MB-231 Breast Cancer Cell Line. *Iran. J. Basic Med. Sci.* **2021**, *24* (7), 928−934.
(80) Huang, L.; Jin, K.; Lan, H. Luteolin Inhibits Cell Cycle Progression and Induces Apoptosis of Breast Cancer Cells through Downregulation of Human Telomerase Reverse Transcriptase. *Oncol. Lett.* **2019**, *17*, 3842−3850.
(81) Robaszkiewicz, A.; Balcerczyk, A.; Bartosz, G. Antioxidative and Prooxidative Effects of Quercetin on A549 Cells. *Cell Biol. Int.* **2007**, *31* (10), 1245−1250.
(82) Cai, X.; Ye, T.; Liu, C.; Lu, W.; Lu, M.; Zhang, J.; Wang, M.; Cao, P. Luteolin Induced G2 Phase Cell Cycle Arrest and Apoptosis on Non-Small Cell Lung Cancer Cells. *Toxicol. in Vitro* **2011**, *25* (7), 1385−1391.
(83) Niazvand, F.; Orazizadeh, M.; Khorsandi, L.; Abbaspour, M.; Mansouri, E.; Khodadadi, A. Effects of Quercetin-Loaded Nanoparticles on MCF-7 Human Breast Cancer Cells. *Medicina* **2019**, *55* (4), 114.
(84) Astolfi, L.; Ghiselli, S.; Guaran, V.; Chicca, M.; Simoni, E.; Olivetto, E.; Lelli, G.; Martini, A. Correlation of Adverse Effects of Cisplatin Administration in Patients Affected by Solid Tumours: A Retrospective Evaluation. *Oncol. Rep.* **2013**, *29* (4), 1285−1292.

https://doi.org/10.1021/acsomega.3c05841
ACS Omega 2023, 8, 40764−40774